Supplement of Atmos. Chem. Phys., 26, 7895–7915, 2026
https://doi.org/10.5194/acp-26-7895-2026-supplement


Atmospheric Chemistry and Physics
Open Access
EGU

*Supplement of*

# Comparing secondary organic aerosols schemes implemented in current chemical transport models and the policy implications of uncertainties

**Ling Huang et al.**

*Correspondence to:* Greg Yarwood (gyarwood@ramboll.com) and Li Li (lily@shu.edu.cn)

## Table of Contents



No. of pages: 35
No. of tables: 23
No. of figures: 5

List of Abbreviations

ALK4 Alkanes $5\times10^3 < k_{OH} < 1\times10^4$ (lumped class)

ALK5 Alkanes $1\times10^4 < k_{OH}$ (lumped class)

ARO1 Aromatics $k_{OH} < 2\times10^4$ (lumped class)

ARO2 Aromatics $k_{OH} > 2\times10^4$ (lumped class)

ASOA SOA formed from AVOC

AVOC Anthropogenic VOC

BENZ Benzene (explicit)

BSOA SOA formed from BVOC

BVOC Biogenic VOC

CG Condensable gases

CTM Chemical transport model

HUMULE Humulene (lumped sesquiterpenes class)

ISOP Isoprene (explicit)

IVOC Intermediate volatility organic compounds

IV-SOA SOA formed from IVOC

LIMO Limonene (lumped class)

OA Organic aerosol

OLE1 Alkenes $k_{OH} < 7\times10^4$ (lumped class)

OLE2 Alkenes $k_{OH} > 7\times10^3$ (lumped class)

POA Primary organic aerosol

$PM_{2.5}$ Particulate matter with a diameter of 2.5 micrometers or less

SESQ Sesquiterpenes (lumped class)

SOA Secondary organic aerosol

SVOC Semivolatile organic compounds

TERP Terpenes (lumped class)

TOL Toluene (lumped class)

VOC Volatile organic compounds

VBS Volatility basis set

XYL Xylenes (lumped class)

## Section S1 Parameterization of SOA scheme in different CTMs

### S1.1 CAMx

The Comprehensive Air quality Model with Extensions (CAMx; Emery et al., 2024) is an Eulerian CTM developed and distributed by Ramboll and version 7.20 was released on May 2nd, 2022 (https://www.camx.com/, accessed on Feb 15th, 2024). CAMx provides two options to simulate SOA chemistry/partitioning: a "two-product" semi-volatile equilibrium scheme called SOAP (Strader et al., 1999) and a hybrid 1.5-dimension volatility basis set (1.5-D VBS) approach (Koo et al., 2014). The former is compatible with advanced probing tools, including the Particulate Source Apportionment Technology (PSAT) and the decoupled direct method (DDM), while the latter is not.

#### *S1.1.1 CAMx SOAP2*

In the CAMx SOAP scheme version 2 (SOAP2), POA is treated as non-volatile and does not chemically evolve. SOA formation is represented by a modified "two product" model described above (Figure 1), where gas-phase VOC and IVOC are oxidized to CGs that can condense to SOA. SOAP2 modifies the two-product scheme by adding a third product, which is considered non-volatile and always condenses to SOA. The CG products from anthropogenic and biogenic precursors have different volatilities in SOAP2. Thus, SOAP2 includes 6 product species overall, as shown in Table S1. The SOA mass yields do not differentiate between different oxidants (i.e., OH, $O_3$, and $NO_3$) in SOAP2 and the yield coefficients are fitted to aged SOA yields (Hodzic et al., 2016). Therefore, no further aging is included in SOAP2. However, SOA is destroyed in the particle phase by photolysis at a rate of $0.1\% \times J_{NO2}$ ($NO_2$ photolysis rate). Aqueous-phase formation of non-volatile SOA from glyoxal and methylglyoxal is also included with SOAP2.

**Table S1** Parameters for SOA formation in CAMx SOAP2 modified two-product scheme (adapted from Table 5-5 of Ramboll, 2022)

| | | | |
|---|---|---|---|
| *SOA mass-based yields (g/g) from anthropogenic precursors under low (top) / high (bottom) NOx conditions* | | | |
| C* [μg/m$^3$] @ 300K | 0 | 0.31 | 14 |
| CG/SOA MW [g/mol] | 220 | 150 | 160 |
| $\Delta H_{vap}$ [kJ/mol] | - | 147 | 116 |
| Benzene | 0 | 0.167 | 0.487 |
| | 0 | 0.391 | 0.248 |
| Toluene | 0.262 | 0.345 | 0.663 |
| | 0.044 | 0.293 | 0.304 |
| Xylene | 0.294 | 0.306 | 0.291 |
| | 0.025 | 0.049 | 0.084 |
| IVOC | 0.277 | 0.275 | 0 |
| | 0.129 | 0.225 | 0.012 |
| *SOA mass-based yields (g/g) from biogenic precursors under low (top) / high (bottom) NOx* | | | |
| C* [μg/m$^3$] @ 300K | 0 | 0.45 | 26 |
| CG/SOA MW [g/mol] | 220 | 180 | 180 |
| $\Delta H_{vap}$ [kJ/mol] | - | 123 | 118 |
| Isoprene | 0.011 | 0.029 | 0.156 |
| | 0 | 0.023 | 0.076 |
| Monoterpene | 0.070 | 0.090 | 0.150 |
| | 0.070 | 0.045 | 0.075 |
| Sesquiterpene | 0.270 | 0.400 | 0.136 |
| | 0.175 | 0.328 | 0.092 |

### *S1.1.2 CAMx VBS*

The CAMx hybrid VBS approach, called 1.5-D VBS, combines the simplicity of 1-D VBS (Donahue et al. 2006; Robinson et al. 2007) with the ability to describe the evolution of OA in both dimensions of oxidation state and volatility (Koo et al. 2014). Unlike SOAP2, CAMx 1.5-D VBS treats POA as semi-volatile, and uses two basis sets with five volatility bins (C* ranging from $10^{-1}$ to $10^3$ μg/m$^3$ at 298K) to describe SOA formation from anthropogenic and biogenic precursors, respectively. Gas-phase oxidation products in different bins are continuously oxidized by OH (with a rate constant $k_{OH}$ of $2\times10^{-11}$ cm$^3$ molecule$^{-1}$ s$^{-1}$) that move mass from higher volatility bins to the next lower volatility bin in a step-wise manner (for example, from C*=1000 μg/m$^3$ to C*=100 μg/m$^3$ and from C*=100 μg/m$^3$ to C*=10 μg/m$^3$, as

illustrated by Figure 2b). For biogenic SOA, this step-wise aging is disabled because over-prediction of OA in rural areas was reported (Lane et al., 2008; Murphy and Pandis, 2009). Like SOAP2, SOA is destroyed by particle-phase photolysis at a rate of $0.1\% \times J_{NO2}$. Table S2 shows the parameters used for the CAMx 1.5-D VBS scheme. The SOA yields from $NO_3$-initiated monoterpene oxidation are different from OH-initiated oxidation and the SOA yields for monoterpenes and IVOC are NO*x*-independent. CAMx 1.5-D VBS differentiates SOA yields from different IVOC sources: gasoline engines (IVOG), diesel engines (IVOD), biomass burning (IVOB), and other anthropogenic sources (IVOA). SOA yields for IVOD, IVOB and IVOA are the same and we only present results for IVOA in this study. Aqueous-phase formation of non-volatile SOA from glyoxal and methylglyoxal is also included in the CAMx 1.5D VBS.

**Table S2** Parameters for SOA formation in CAMx 1.5-D VBS (values adopted from CAMx source code)

| C* [μg/m$^3$] @ 298K | 0 | 1 | 10 | 100 | 1000 |
|---|---|---|---|---|---|
| CG/SOA MW [g/mol] | 172 | 167 | 163 | 158 | 153 |
| $\Delta H_{vap}$ [kJ/mol] | 35 | 35 | 35 | 35 | 35 |
| *SOA molar yield (ppm/ppm) under high (top)/low (bottom) NOx* | | | | | |
| Benzene | 0 | 0.001 | 0.079 | 0.148 | 0.222 |
| | 0 | 0.035 | 0.108 | 0.185 | 0.268 |
| Toluene | 0 | 0.006 | 0.145 | 0.281 | 0.432 |
| | 0 | 0.006 | 0.145 | 0.437 | 0.281 |
| Xylene | 0 | 0.001 | 0.127 | 0.201 | 0.301 |
| | 0 | 0.048 | 0.195 | 0.252 | 0.364 |
| Isoprene | 0 | 0 | 0.009 | 0.006 | 0 |
| | 0 | 0.004 | 0.013 | 0.006 | 0 |
| Monoterpenes | 0 | 0.01 | 0.101 | 0.173 | 0.451 |
| | 0 | 0.087 | 0.077 | 0.309 | 0.54 |
| Sesquiterpenes | 0 | 0.092 | 0.188 | 0.968 | 0.679 |
| | 0 | 0.092 | 0.188 | 0.968 | 0.679 |
| *SOA molar yield (ppm/ppm) for IVOC* | | | | | |
| IVOG | 0.022 | 0.098 | 0.373 | 0.699 | 0 |
| IVOD | 0.081 | 0.135 | 0.800 | 0.604 | 0 |
| IVOA | 0.081 | 0.135 | 0.800 | 0.604 | 0 |
| IVOB | 0.081 | 0.135 | 0.800 | 0.604 | 0 |
| *SOA molar yield (ppm/ppm) for $NO_3$ oxidation* | | | | | |
| Monoterpenes | 0.314 | 0.029 | 0 | 0.862 | 0 |

## S1.2 CMAQ

The Community Multiscale Air Quality (CMAQ) model is developed and distributed by the US Environmental Protection Agency (EPA). The version CMAQ v5.4 released in October 2022 offers three SOA options: AERO7 inherited from earlier versions (Appel et al., 2021), CRACMM (Pye et al., 2023) introduced in v5.4 for the first time, and a 2D-VBS developed by Tsinghua University (https://github.com/USEPA/CMAQ/tree/2DVBS, accessed Feb 15th, 2024). We reviewed the first two schemes because both were developed by EPA to support air quality planning in the U.S. and elsewhere.

### *S1.2.1 CMAQ AERO7*

The CMAQ AERO7 introduced in version 5.3 (Appel et al. 2021) tracks SOA formation from anthropogenic VOC (benzene, alkanes, aromatics, polycyclic aromatic hydrocarbons (PAHs)), biogenic VOC (isoprene, α-pinene, monoterpenes, and sesquiterpenes), and IVOC. Additionally, AERO7 accounts for in-cloud SOA formation from glyoxal and methylglyoxal and aerosol aqueous-phase SOA formation from glyoxal, methylglyoxal and isoprene epoxydiols (IEPOX). AERO7 scheme employs VBS-based approaches to represent SOA yields from different precursors, with varying volatility ranges for each precursor. Table S3 to Table S5 list the AERO7 SOA yields for precursors considered in this study. Specifically, AERO7 uses a VBS approach with four bins ($C^*$ ranging from 0.01 μg/m$^3$ to 100 μg/m$^3$ at 298K, Table S3) to represent SOA formation from anthropogenic VOC precursors (e.g., benzene, long alkanes, PAHs, Table S3) and seven bins ($C^*$ ranging from 0.01 to $10^7$ μg/m$^3$ at 298K, Table S4) for α-pinene and monoterpenes. Isoprene and sesquiterpene oxidation products are parameterized with two and one semivolatile products (Table S5), respectively. IVOC in CMAQ is represented by model species pcVOC, which oxidizes with OH to form a low-volatility condensable vapor (pcSOG, $C^*=10^{-5}$ μg/m$^3$) with a molar yield of 1 (Murphy et al. 2017, Table S5).

AERO7 incorporates aging treatments for SOA that vary by precursor as detailed in

Table S6. SOA formed from AVOC, isoprene, and sesquiterpenes undergo oligomerization in the particle-phase to form non-volatile SOA (as illustrated by Figure 2d) with a static rate constant $k_{OLIG}$ of $9.49\times10^{-6}$ $s^{-1}$ (equivalent to a lifetime of ~30 hr). In contrast, no oligomerization occurs for SOA formed from OH-initiated monoterpene oxidation, while SOA formed from $NO_3$-initiated monoterpene oxidation is subject to particle-phase hydrolysis to non-volatile SOA with a rate constant of $9.25\times10^{-5}$ $s^{-1}$ (equivalent to a lifetime of 3 hr). Unlike CAMx, SOA photolysis is not considered in AERO7.

**Table S3** Parameters for SOA formation from aromatics under high- (top row) and low- (bottom row) NO*x* conditions in CMAQ AERO7

| C* [µg/m$^3$] @ 298K | 0.01 | 1 | 10 | 100 |
|---|---|---|---|---|
| ΔHvap [kJ/mol] | 18 | 18 | 18 | 18 |
| CG/SOA MW [g/mol] | 198 | 179 | 169 | 158 |
| Precursor | SOA molar yields | | | |
| Benzene | 0 | 0.034 | 0 | 0.392 |
| | 0.146 | 0 | 0 | 0 |
| Toluene | 0 | 0.016 | 0.051 | 0.047 |
| | 0.14 | 0 | 0 | 0 |
| Xylene | 0 | 0.015 | 0.023 | 0.06 |
| | 0.193 | 0 | 0 | 0 |

**Table S4** Parameters for SOA formation from monoterpenes and $\alpha$-pinene in CMAQ AERO7

| C* [µg/m$^3$] @ 298K | 0.01 | 0.1 | 1 | 10 | 100 | 1000 | 10000 |
|---|---|---|---|---|---|---|---|
| ΔHvap [kJ/mol] | 102 | 91 | 80 | 69 | 58 | 47 | 36 |
| CG/SOA MW [g/mol] | 300 | 200 | 186 | 184 | 170 | 168 | / |
| SOA molar yields | 0.040 | 0.032 | 0.032 | 0.103 | 0.143 | 0.285 | 0.160 |

**Table S5** Parameters for SOA formation from isoprene, sesquiterpenes, and IVOC in CMAQ AERO7

| Precursor | Isoprene | | Sesquiterpenes | IVOC |
|---|---|---|---|---|
| C* [µg/m$^3$] @ 298K | 0.617 | 116.01 | 24.984 | 1E-05 |
| ΔHvap [kJ/mol] | 40 | 40 | 40 | 40 |
| CG/SOA MW [g/mol] | 132 | 133 | 273 | 170 |
| SOA mass yields | 0.0288 | 0.232 | 1.537 | 1.176 |

**Table S6** Aging effect for different SOA precursors in CMAQ AERO7

| SOA precursors | Aging effect treatment |
|---|---|
| Aromatics | Under high-NO*x* conditions, oxidation products form non-volatile oligomers (AOLGA) at a rate of $9.49\times10^{-6}$ $s^{-1}$; under low-NO*x* conditions, oxidation products do not form oligomers, i.e., no aging effect. |
| Isoprene/Sesquiterpene | Aging is NO*x*-independent; oxidation products form non-volatile oligomers (AOLGB) at a rate of $9.49\times10^{-6}$ $s^{-1}$ |
| Monoterpenes | There is no aging effect for OH and $O_3$ oxidation products; $NO_3$ oxidation products undergo hydrolysis to form a non-volatile product (AMTHYD) at a rate of $9.26\times10^{-5}$ $s^{-1}$ |
| IVOC | No aging effect |

***S1.2.2*** CMAQ CRACMM

The Community Regional Atmospheric Chemistry Multiphase Mechanism (CRACMM) was introduced in CMAQv5.4 (Pye et al., 2023). Unlike other SOA schemes, CRACMM partially integrates CG formation and CG aging with oxidant formation in the gas-phase chemical mechanism. Consequently, SOA formation occurs through multiple sequential reactions (as illustrated below for benzene), meaning that the SOA yield parameters are too complex to be tabulated for CRACMM in contrast to the other schemes reviewed here. CRACMM SOA formation considers a comprehensive range of reactive organic carbon (ROC) precursors, including alkane-like ROC, aromatics, furans, isoprene, monoterpenes, sesquiterpenes, glyoxal and methylglyoxal. Furthermore, CRACMM categorizes IVOC based on functional groups to aromatic IVOC, oxygenated IVOC, and alkane IVOC. Aqueous SOA formation from IEPOX, glyoxal, and methylglyoxal follow CMAQ AERO7.

SOA formation from the OH-initiated oxidation of benzene (BENZ in CRACMM) is shown here as an example where only the SOA-related products are identified (SR1 to SR5):

$$\mathrm{BENZ + OH \rightarrow 0.470\ BENP + 0.530\ PHEN + \ldots} \qquad \text{SR1}$$

$$\text{BENP} + \text{NO} \rightarrow 0.001\ \text{VROCP4OXY2} + 0.001\ \text{VROCN1OXY6} + 0.499\ \text{FURANONE} + \ldots \quad \text{SR2}$$

$$\text{BENP} + \text{HO2} \rightarrow 0.398\ \text{VROCN1OXY6} + \ldots \quad \text{SR3}$$

$$\text{FURANONE} + \text{OH} \rightarrow 0.040\ \text{ASOATJ} + \ldots \quad \text{SR4}$$

$$\text{PHEN} + \text{OH} \rightarrow 0.152\ \text{ASOATJ} + \ldots \quad \text{SR5}$$

Non-volatile products (e.g. ASOATJ in this example) always form 100% SOA. In contrast, semi-volatile products (e.g. VROCP4OXY2 and VROCN1OXY6) can react further with OH in the gas-phase and undergo functionalization and/or fragmentation within a simplified 2-D VBS. By employing a straightforward application of linear algebra, we can multiply the stoichiometric coefficients of sequential reaction steps (i.e., SR1 to SR5 for benzene) under both high and low NO*x* conditions. This approach results in SOA yields that align closely with the values of Pye et al. (2023) for the average of high and low NO*x* conditions. However, this algebraic calculation assumes 100% reaction of the precursor and all intermediate products, such as phenol (PHEN) and furanone. In reality, intermediate products react sequentially with varying reaction rates (e.g., SR3 to SR7) that are influenced by the concentrations of OH, $HO_2$ or NO. For illustration, we present detailed calculations of aged SOA formation for CRACMM benzene and α-pinene in Section S2. As shown by these calculations, the non-aged SOA yields in CRACMM are zero and thus were excluded from the discussion of non-aged yields in Section 4.1. As the reactions progress, however, SOA yields begin to rise, demonstrating the importance of aging to CRACCM. Like CMAQ AERO7, SOA photolysis is not accounted for in CRACMM.

### S1.3 GEOS-Chem

GEOS-Chem is a global chemical transport model driven by meteorological input from the Goddard Earth Observing System (GEOS) of the NASA Global Modeling and Assimilation Office (https://zenodo.org/records/10640536, accessed on March 1st, 2024). GEOS-Chem is widely used for studying air quality and atmospheric

chemistry. Two SOA schemes are available within GEOS-Chem: a simple scheme and a complex scheme (hereafter GEOS-Chem Simple and GEOS-Chem Complex) as described by Pai et al. (2020). The former provides computationally efficient SOA estimates by treating all SOA as non-volatile and using anthropogenic CO emissions as a surrogate for all anthropogenic SOA precursor emissions. The latter implements a conventional 1-D VBS framework. The GEOS-Chem Simple scheme is interesting because it has been shown to replicate atmospheric measurements more successfully than complex schemes with many more parameters (Nault et al., 2021).

### *S1.3.1 GEOS-Chem Simple scheme*

The GEOS-Chem Simple scheme converts a single lumped anthropogenic SOA (ASOA) precursor to non-volatile SOA with a constant lifetime of 1 day and 100% yield. The anthropogenic precursor emissions are estimated using CO emissions as a proxy, with scaling factors of 1.3% and 6.9% for fire/biofuel and fossil fuel sources respectively. This scheme (Hodzic and Jimenez, 2011; Nault et al., 2021) was developed by comparing ambient measurements of SOA with CO, which confounds the assumed ASOA yield (100%) with the derived anthropogenic precursor emission scaling factors (1.3% or 6.9%). Consequently, we exclude the Simple scheme ASOA yields from some comparisons with other schemes presented below because the assumption of 100% yield could be considered arbitrary. SOA formation from IVOC is not explicitly considered in the GEOS-Chem Simple scheme. For BVOC, the Simple scheme assumes formation of non-volatile biogenic SOA (BSOA) with constant yields of 3% for isoprene and 10% for monoterpenes and sesquiterpenes. 50% of the BSOA is formed promptly and the remaining 50% is formed with a constant lifetime of 1.15 days. The Simple scheme has no treatment of SOA aging or SOA photolysis.

### *S1.3.2 GEOS-Chem Complex scheme*

The GEOS-Chem complex scheme represents SOA formation from anthropogenic and biogenic precursors using a VBS framework. The SOA yields from OH and $O_3$ initiated oxidation are listed in Table S7 (Pye et al., 2010). This scheme does not include further aging processes (e.g. Figure2a) and our review of the source code

found no treatment of SOA photolysis. SOA formation from IVOC is simulated using naphthalene as a proxy. Additionally, irreversible SOA formation occurs from the aqueous-phase reactive uptake of isoprene (Marais et al., 2016), which is outside the primary focus of the current study.

**Table S7** SOA yield[1] parameterization of GEOS-Chem Complex scheme (adopted from Pye et al. 2010)

| C* [μg/m3] @ 298K | Mass yields (g/g) under high (top)/low (bottom) NO*x* conditions | | | | | $\Delta H_{vap}$ [kJ/mol] |
|---|---|---|---|---|---|---|
| | Non-volatile | 0.1 | 1 | 10 | 100 | |
| ISOP | 0 | 0 | 0.0306 | 0.0000 | 0.0945 | 42 |
| MTPA[2] | 0 | 0.04 | 0.0095 | 0.0900 | 0.0150 | 42 |
| | 0 | 0.08 | 0.0190 | 0.1800 | 0.0300 | |
| LIMO | 0 | 0 | 0.4743 | 0.1174 | 1.4190 | 42 |
| | 0 | 0 | 0.3661 | 0.3214 | 0.8168 | |
| SESQ | 0 | 0 | 0.0005 | 1.1463 | 2.9807 | 42 |
| | 0 | 0 | 0.0000 | 0.5738 | 1.4893 | |
| BENZ | 0 | 0 | 0.0778 | 0.0000 | 0.7932 | 42 |
| | 0.37 | 0 | 0.0000 | 0.0000 | 0.0000 | |
| TOL | 0 | 0 | 0.0315 | 0.0944 | 0.0800 | 42 |
| | 0.30 | 0 | 0 | 0.0000 | 0.0000 | |
| XYL | 0 | 0 | 0.0250 | 0.0360 | 0.0899 | 42 |
| | 0.36 | 0 | 0 | 0.0000 | 0.0000 | |
| IVOC[3] | 0 | 0 | 0.0390 | 0.2960 | 0.2350 | 42 |
| | 0.73 | 0 | 0 | 0.0000 | 0.0000 | |

[1]SOA yield for OH and $O_3$ oxidation. SOA yields from $NO_3$ oxidation with isoprene and terpenes are not presented in this table.
[2] α-pinene and similar monoterpenes
[3] Use naphthalene as a proxy

## S1.4 CHIMERE

CHIMERE is an Eulerian chemistry-transport model widely used for operational regional air quality forecasts (Honore et al. 2008) and research in Europe (Beekmann and Vautard, 2010; Sciare et al., 2010) as well as other regions of the world (Zhang et al., 2012; Hodzic et al., 2009, 2010; Ma et al., 2019). Version v2023r1 was released in December 2023. Within CHIMERE, three SOA formation schemes are available: single-step oxidation, the Hydrophilic/Hydrophobic Organics ($H_2O$) mechanism (Couvidat et al., 2018), and a VBS scheme (Zhang et al., 2013; Cholakian et al., 2018). The VBS scheme includes two subsets: one involving only

functionalization and the other involving functionalization, fragmentation, and oligomerization (Zhang et al. 2013; Shrivastava et al. 2015).

We reviewed the CHIMERE VBS scheme with functionalization, fragmentation, and oligomerization processes, referred to as CHIMERE VBS. This scheme models SOA precursors using the SAPRC99 VOC lumping scheme (Luecken et al., 2008) and four VBS bins (C* ranging 1 to $10^3$ μg/m$^3$ at 298K) with corresponding SOA mass yields listed in Table S8 (Zhang et al. 2013; CHIMERE, 2023). The aging processes for AVOC and BVOC are slightly different in CHIMERE VBS but basically follow Figure2c. For AVOC, the first two generations of gas-phase products undergo OH-initiated functionalization oxidation with a 7.5% mass gain to account for oxygen addition:

$$ASOA_n(g) + OH \rightarrow 1.075*ASOA_{n-1}(g) \quad \text{SR6}$$

Subsequent generations undergo both functionalization (15% yield adjusted for oxygen mass gain) and fragmentation (75%):

$$ASOA_n(g) + OH \rightarrow 0.16125*ASOA_{n-1}(g) + 0.75*ASOA_4(g) \quad \text{SR7}$$

Subscript 4 represents the most volatile bin (C*=$10^3$ μg/m$^3$ at 298K). Implicitly, SR7 assumes a 10% yield of volatile products such as CO or $CO_2$. For BVOC, the fragmentation process occurs from the first generation:

$$BSOA_n(g) + OH \rightarrow 0.16125*BSOA_{n-1}(g) + 0.75*BSOA_4(g) \quad \text{SR8}$$

In the CHIMERE VBS scheme, both functionalization and fragmentation occur with an OH rate constant $k_{OH}$ of $1\times10^{-11}$ cm$^3$ molecule$^{-1}$ s$^{-1}$. Non-volatile SOA (i.e., ANVSOA and BNVSOA) is formed by oligomerization with a rate constant $k_{OLIG}$ of $3\times10^{-4}$ s$^{-1}$ corresponding to a lifetime of 1 hr (SR9 and SR10).

$$ASOA_n(p) \rightarrow ANVSOA \quad \text{SR9}$$

$$BSOA_n(p) \rightarrow BNVSOA \quad \text{SR10}$$

CHIMERE represents IVOC using three high volatility bins of the POA VBS (POA7 to POA9, corresponding to $C^* = 10^4$ to $10^6$ μg/m$^3$). The IVOC mass fraction assigned to each bin is 24%, 29%, and 47% (Zhang et al. 2013). The gas-phase fraction of each volatility bin undergoes OH-initiated oxidation to form oxidized

POA (OPOA) with lower and/or higher volatility. Similar to ASOA formation, the first two generations of IV-SOA (SOA formed from IVOC) undergo only functionalization reactions (with a 7.5% mass gain, SR11) while subsequent generations undergo both functionalization (15% goes to the next lower volatility bin) and fragmentation (75% goes to the next higher volatility bin, SR12):

$$POA_n\ (g) + OH \rightarrow 1.075\ OPOA_{n-1}\ (g) \qquad SR11$$

$$POA_n\ (g) + OH \rightarrow 0.16125\ OPOA_{n-1}\ (g) + 0.75\ OPOA_{n+1}\ (g) \qquad SR12$$

**Table S8** SOA yield parameterization in CHIMERE VBS (Zhang et al., 2013; CHIMERE, 2023)

| C* [μg/m$^3$] @ 300K | Mass yields under high (top)/low (bottom) NO*x* conditions (molar-based)[2] | | | | $\Delta H_{vap}$ [kJ/mol] | CG/SOA MW [g/mol] |
|---|---|---|---|---|---|---|
| | 1 | 10 | 100 | 1000 | | |
| ISOP | 0.0003 | 0.0225 | 0.015 | 0 | 30 | 180 |
| | 0.009 | 0.03 | 0.015 | 0 | | |
| TERP[1] | 0.012 | 0.1215 | 0.201 | 0.507 | 30 | 180 |
| | 0.1073 | 0.0918 | 0.3587 | 0.6075 | | |
| HUMULE | 0.075 | 0.15 | 0.75 | 0.9 | 30 | 180 |
| | 0.075 | 0.15 | 0.75 | 0.9 | | |
| ARO1 | 0.003 | 0.165 | 0.3 | 0.435 | 30 | 150 |
| | 0.075 | 0.225 | 0.375 | 0.525 | | |
| ARO2 | 0.0015 | 0.195 | 0.3 | 0.435 | 30 | 150 |
| | 0.075 | 0.3 | 0.375 | 0.525 | | |
| ALK4 | 0 | 0.0375 | 0 | 0 | 30 | 120 |
| | 0 | 0.075 | 0 | 0 | | |
| ALK5 | 0 | 0.15 | 0 | 0 | 30 | 150 |
| | 0 | 0.3 | 0 | 0 | | |
| OLE1 | 0.0008 | 0.0045 | 0.0375 | 0.15 | 30 | 120 |
| | 0.0045 | 0.009 | 0.06 | 0.225 | | |
| OLE2 | 0.003 | 0.0225 | 0.0825 | 0.27 | 30 | 120 |
| | 0.0225 | 0.0435 | 0.129 | 0.375 | | |

[1] Same mass yields are used for APINEN, BPINEN, OCIMEN, and LIMONE. Use TERP to represent all monoterpene species.

[2] Yields for OH and $O_3$ oxidation are the same for biogenic VOCs.

## S1.5 WRF-Chem

WRF-Chem adds atmospheric chemistry to the Weather Research and Forecasting (WRF) meteorological model to simulate interactions between meteorology and atmospheric chemistry. Version v4.4 released in April 2022 offers five aerosol

schemes (WRF-Chem, 2022): 1) Modal Aerosol Dynamics Model for Europe (MADE/SORGAM, Schell et al. 2001), 2) Modal Aerosol Dynamics Model for Europe with the VBS (MADE/VBS), 3) Modal Aerosol Module (MAM), 4) Model for Simulating Aerosol Interactions and Chemistry (MOSAIC) sectional model aerosol parametrization, and 5) bulk aerosol module from GOCART.

We reviewed the MOSAIC scheme as an example of a VBS scheme with functionalization and fragmentation. In the MOSAIC scheme (Shrivastava et al. 2011), SOA formation from OH-oxidation is considered but reactions with $O_3$ and $NO_3$ radicals are not included. The formation of SOA from both AVOC and BVOC is modeled using a 4-bin VBS (C* ranging from 0.1 to 100 $\mu g/m^3$ at 298K) with constant yields (

Table **S9**). No additional aging processes are considered for the condensable gases. SOA photolysis is included in the source code but turned off by default.

In WRF-Chem, IVOC is represented by three bins, with $C^*$ ranging from $10^4$ to $10^6$ $\mu g/m^3$. The formation of SOA from IVOC involves OH-oxidation of both the non-oxygen (with subscript c) and oxygen parts (with subscript o), with a first-order rate constant $k_{OH}$ of $4\times10^{-11}$ $cm^3$ $molecule^{-1}$ $s^{-1}$. For the non-oxygen part, oxidation results in formation of non-oxygen and oxygen parts (with 15% mass gain) with lower volatility (SR13 and SR14). At the same time, the oxygen parts oxidize with OH and move to a lower volatility bin (SR15 and SR16). Therefore, at any time both non-oxygen and oxygen parts move to successively lower volatility bins. The lowest volatility species ($C^*$ = 0.01 $\mu g/m^3$) are assumed to be inert and have no fragmentation reactions.

$$IVOC_{n,\,c}(g) + OH \rightarrow SOA_{n-1,c}(g) + 0.15*SOA_{n-1,o}(g) \quad \text{SR13}$$

$$SOA_{n,\,c}(g) + OH \rightarrow SOA_{n-1,c}(g) + 0.15*SOA_{n-1,o}(g) \quad \text{SR14}$$

$$IVOC_{n,\,o}(g) + OH \rightarrow SOA_{n-1,o}(g) \quad \text{SR15}$$

$$SOA_{n,\,o}(g) + OH \rightarrow SOA_{n-1,o}(g) \quad \text{SR16}$$

307 **Table S9 SOA** yield (g/g) parameterization of WRF-Chem MOSAIC (adopted
308 from Shrivastava et al. 2011).

| C* (µg/m$^3$) @ 298K | Mass yields (g/g) of each bin under high (top)/low (bottom) NO*x* conditions | | | | MW [g/mol] |
|---|---|---|---|---|---|
| | 1 | 10 | 100 | 1000 | |
| ISOP | 0.001 | 0.023 | 0.015 | 0 | 250 |
| | 0.009 | 0.03 | 0.15 | 0 | |
| TERP | 0.012 | 0.122 | 0.201 | 0.5 | 250 |
| | 0.107 | 0.092 | 0.359 | 0.6 | |
| SESQ | 0.075 | 0.15 | 0.75 | 0.9 | 250 |
| | 0.075 | 0.15 | 0.75 | 0.9 | |
| ARO1 | 0.01 | 0.24 | 0.45 | 0.7 | 250 |
| | 0.01 | 0.24 | 0.7 | 0.7 | |
| ARO2 | 0.01 | 0.24 | 0.45 | 0.7 | 250 |
| | 0.01 | 0.24 | 0.7 | 0.7 | |
| ALK4 | 0 | 0.38 | 0 | 0 | 250 |
| | 0 | 0.075 | 0 | 0 | |
| ALK5 | 0 | 0.15 | 0 | 0 | 250 |
| | 0 | 0.3 | 0 | 0 | |
| OLE1 | 0.001 | 0.005 | 0.038 | 0.15 | 250 |
| | 0.005 | 0.009 | 0.06 | 0.225 | |
| OLE2 | 0.003 | 0.026 | 0.083 | 0.27 | 250 |
| | 0.023 | 0.044 | 0.129 | 0.375 | |

## Section S2 An example of offline calculation for the SOA yields

As an illustrative example, we present the calculation of non-aged SOA yields from benzene under high NO*x* conditions for the CAMx SOAP2 and CMAQ AERO7 schemes. For CAMx SOAP2, the effective saturation concentration ($C^*$ = 0.31, 14 μg/m$^3$) listed in Table S1 are defined at 300K. These values were adjusted to a standard temperature of 298 K using the Clausius-Clapeyron equation:

$$C_i^* = C_{i,0}^* \frac{T_0}{T} \exp\left[\frac{\Delta H_i^{vap}}{\mathrm{R}}\left(\frac{1}{T_0} - \frac{1}{\mathrm{T}}\right)\right]$$

where $C_i^*$ and $C_{i,0}^*$ are the saturation concentrations for volatility bin *i* at T and $T_0$ (=298 K), respectively. R is the universal gas constant, and $\Delta H_i^{vap}$ denotes the enthalpy of vaporization for volatility bin *i*.

Subsequently, using Eq. 1 and the stoichiometric coefficients from Table S1, the SOA yield from BENZ at $C_{OA}$ of 10 μg/m$^3$ was calculated as:

$$\mathrm{Y} = \frac{0.391}{1 + 0.21/10} + \frac{0.248}{1 + 10.31/10} = 0.505\ g/g$$

The CMAQ AERO7 scheme parameterizes SOA yields from BENZ using a VBS framework. The molar yields listed in Table S3 were converted to mass yields using the molecular of BENZ (=78.1 g/mol) and the oxidation product. Utilizing Eq.2, the SOA yield from BENZ at $C_{OA}$ of 10 μg/m$^3$ was calculated as:

$$\mathrm{Y} = \frac{0.0779}{1 + 1/10} + \frac{0}{1 + 10/10} + \frac{0.793}{1 + 100/10} + \frac{0}{1 + 1000/10} = 0.143\ g/g$$

These calculations were repeated over a $C_{OA}$ range of 0.1 μg/m$^3$ to 50 μg/m$^3$ to generate the yield curves presented in Figure 3. A spreadsheet demonstrating these example calculations is available at https://doi.org/10.5281/zenodo.16757660. Calculation data for other species and schemes are available from the corresponding authors upon request.

## Section S3 Offline calculation of SOA yields in CMAQ CRACMM

In this section, we show how SOA yields from benzene and α-pinene are calculated under high and low NO*x* conditions in CMAQ CRACMM. All the relevant reactions and parameters (

Table **S10**) are obtained from Table B1 and Table S1 of Pye et al. (2023).

### S3.1 SOA yields from benzene

Under high-NO*x* conditions, the following reactions take place that form SOA from benzene (BENZ). For clarity, only the relevant species involved in SOA formation are listed.

| | |
|---|---|
| BENZ + HO → 0.470 BENP + 0.530 PHEN + … | SR17 ($k = 1.22\times10^{-12}$) |
| BENP + NO → 0.001 VROCP4OXY2 + 0.001 VROCN1OXY6 + 0.499 FURANONE + … | SR18 ($k = 9.03\times10^{-12}$) |
| FURANONE + HO → 0.040 ASOATJ + … | SR19 ($k = 4.4\times10^{-11}$) |
| PHEN + HO → 0.152 ASOATJ + … | SR20 ($k = 2.63\times10^{-11}$) |

Under low-NO*x* condition, SOA formation from BENZ follows the following reactions:

| | |
|---|---|
| BENZ + HO → 0.470 BENP + 0.530 PHEN + … | SR21 ($k = 1.22\times10^{-12}$) |
| PHEN + HO → 0.152 ASOATJ + … | SR22 ($k = 2.63\times10^{-11}$) |
| BENP + $HO_2$ → 0.398 VROCN1OXY6 + … | SR23 ($k = 2.28\times10^{-11}$) |

In our calculation, we assumed [OH]=$3.0\times10^{6}$ molecules/$cm^3$, [NO]=100 ppt, and [$HO_2$]= $1.5\times10^{8}$ molecules/$cm^3$ (=[OH] × 50) for the calculation of reaction rates. The saturation concentration ($C^*$) for the species VROCP4OXY2, VROCN1OXY6 and ASOATJ is $10^4$, $10^{-1}$ and $10^{-9}$ μg/$m^3$, respectively. With an ambient OA concentration ($C_{OA}$) of 10 μg/$m^3$, the gas fractions of the three species are 100%, 1%, and 0%. VROCP4OXY2 and VROCN1OXY6 participate in further reactions with OH, resulting in products that exhibit either increased or decreased $C^*$, as outlined in Table S10 below (derived from the reactions labeled under "ROCOXY" in Table B1 of Pye et al. (2023)). In contrast, ASOATJ is characterized as non-volatile and non-reactive.

Calculations are stepped through time to simulate aging. At each time step, denoted as *t*, the total SOA mass is the sum of ASOATJ and the particle fraction of semi-volatile species:

$$SOA_t = [ASOATJ]_t + (f_{particle}^{VROCP4OXY2} \times [VROCP4OXY2]_t + f_{particle}^{VROCN1OXY6} \times [VROCN1OXY6]_t + f_{particle}^{VROCN1OXY1} \times [VROCN1OXY1]_t + \cdots)$$ Eq. S1

Where $f_{particle}^{species}$ is the particle fraction of each semi-volatile species and $[species]_t$ represents the mass of species (i.e. VROCP4OXY2, VROCN1OXY6) at time *t*. The mass of ASOATJ at time *t* is further calculated as:

$$[ASOATJ]_t = [ASOATJ]_{t-1} + \sum_n \{[species]|_{t-1}^{j} \times f_{gas}^{j} \cdot (1\text{-}e^{-k_{OH}^{j} * [OH] * \Delta t}) \times \alpha_j^{ASOATJ}\}$$ Eq. S2

*j* represents all the species that, when oxidized by OH, can form ASOATJ and $\alpha_j^{ASOATJ}$ is the corresponding molar yield of ASOATJ. Similarly, the mass of semi-volatile species at time *t*, taking VROCP4OXY2 as an example, is calculated as:

$$[VROCP4OXY2]_t = [VROCP4OXY2]_{t-1} \times (f_{particle}^{VROCP4OXY2} + f_{gas}^{VROCP4OXY2} \cdot e^{-k_{OH} * [OH] * \Delta t}) + \sum_n \{[species]|_{t-1}^{j} \times f_{gas}^{j} \cdot (1\text{-}e^{-k_{OH}^{j} * [OH] * \Delta t}) \times \alpha_j^{VROCP4OXY2}\}$$ Eq. S3

The mass of VROCP4OXY2 at time *t* consists of three components: (1) the particle-phase of VROCP4OXY2 at time *t-1*, (2) the remaining gas-phase of VROCP4OXY2 after OH oxidation, and (3) the additional mass gained from OH oxidation of other species, characterized by molar yields as $\alpha_j^{VROCP4OXY2}$ (as shown in

Table **S10**). We started the calculation from t=0 to t=24 hr and progress with a time step Δt of 0.2 hr. Figure S1a shows the SOA yields from benzene as a function of the aging time. Under both high and low NO*x* conditions, the SOA yields increase sharply during the initial six hours, after which the increase is negligible. With a 24-hour aging period, the SOA yield from benzene is 0.23 g/g under high NO*x* conditions and 0.67 g/g under low NO*x* conditions, respectively.

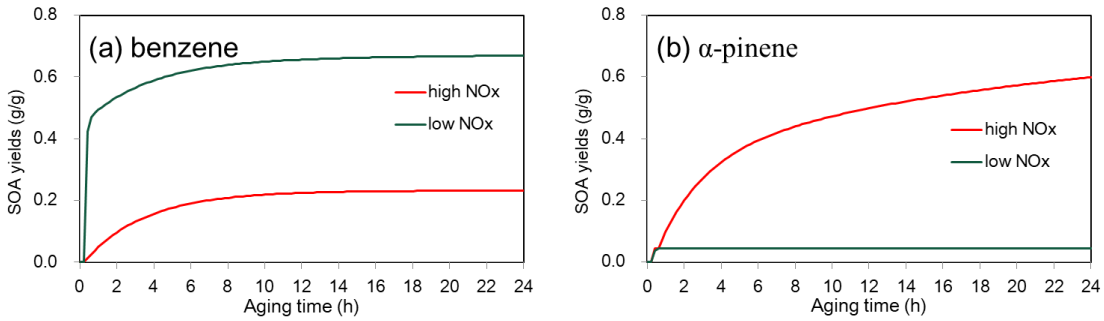


**Figure S1** Effect of OH-oxidation aging on SOA yield (g/g) from (a) benzene and (b) α-pinene as a function of aging time in CMAQ CRACMM.

**Table S10** Stoichiometric yields of L/S/IVOC oxidation by OH (adopted from Table B1 from Pye et al. 2023)

| Species | VROCN2 OXY8 | VROCN2 OXY4 | VROCN2 OXY2 | VROCN1 OXY6 | VROCN1 OXY3 | VROCN1 OXY1 | VROCP0 OXY4 | VROCP0 OXY2 | VROCP1 OXY3 | VROCP1 OXY1 | VROCP2 OXY2 | VROCP3 OXY2 | VROCP4 OXY2 | VROCP5 OXY1 | VROCP6 OXY1 | OP3 |
|---|---|---|---|---|---|---|---|---|---|---|---|---|---|---|---|---|
| C* (μg/m$^3$) | 0.01 | 0.01 | 0.01 | 0.1 | 0.1 | 0.1 | 1 | 1 | 10 | 10 | 100 | 1000 | 10000 | 100000 | 1000000 | 10 |
| $k_{OH}$ | 5.90E-11 | 6.07E-11 | 5.54E-11 | 5.63E-11 | 5.46E-11 | 4.50E-11 | 5.17E-11 | 4.73E-11 | 4.50E-11 | 3.80E-11 | 3.93E-11 | 3.52E-11 | 3.12E-11 | 2.40E-11 | 2.05E-11 | 4.69E-11 |
| VROCN2OXY8 | 0.085 | 0.464 | 0.104 | 0.204 | 0.279 | 0.007 | 0.282 | 0.066 | 0.178 | 0.002 | 0.044 | 0.032 | 0.012 | | | 0.119 |
| VROCN2OXY4 | | 0.198 | 0.564 | 0.007 | 0.403 | 0.119 | 0.117 | 0.458 | 0.192 | 0.134 | 0.173 | 0.076 | 0.017 | 0.01 | | 0.001 |
| VROCN2OXY2 | | | 0.214 | | 0.009 | 0.726 | | 0.116 | 4.00E-04 | 0.335 | 0.01 | 0.001 | | 0.001 | | |
| VROCN1OXY6 | | 0.012 | 0.015 | | 0.032 | 0.012 | 0.032 | 0.033 | 0.074 | 0.008 | 0.051 | 0.053 | 0.048 | 0.009 | 0.006 | 0.039 |
| VROCN1OXY3 | | 0.015 | 0.03 | | 0.008 | 0.03 | 0.018 | 0.066 | 0.045 | 0.119 | 0.112 | 0.049 | 0.025 | 0.015 | 0.005 | |
| VROCN1OXY1 | | | 0.01 | | | 0.007 | | 0.005 | | 0.076 | 0.001 | | | | | |
| VROCP0OXY4 | | 0.062 | 0.019 | | 0.019 | 0.029 | 0.001 | 0.031 | 0.063 | 0.029 | 0.134 | 0.155 | 0.088 | 0.07 | 0.022 | 0.011 |
| VROCP0OXY2 | | | 0.046 | | 0.01 | 0.045 | | 0.002 | 0.001 | 0.077 | 0.04 | 0.015 | | 0.015 | | |
| VROCP1OXY3 | | 0.039 | 0.031 | | 0.051 | 0.023 | | 0.04 | 0.001 | 0.028 | 0.051 | 0.105 | 0.092 | 0.104 | 0.05 | |
| VROCP1OXY1 | | | 0.02 | | 0.007 | 0.035 | | 0.021 | | 0.012 | 0.007 | 0.001 | 0.007 | 0.003 | 0.002 | |
| VROCP2OXY2 | | 0.049 | 0.046 | | 0.051 | 0.062 | 0.066 | 0.054 | 0.023 | 0.065 | 0.024 | 0.053 | 0.097 | 0.165 | 0.088 | |
| VROCP3OXY2 | | 0.04 | 0.045 | | 0.046 | 0.052 | 0.053 | 0.052 | 0.059 | 0.071 | 0.029 | 0.009 | 0.046 | 0.157 | 0.138 | |
| VROCP4OXY2 | | 0.018 | 0.045 | | 0.051 | 0.051 | 0.025 | 0.052 | 0.065 | 0.067 | 0.073 | 0.043 | 0.002 | 0.072 | 0.146 | |
| VROCP5OXY1 | | | 0.033 | | 0.014 | 0.035 | | 0.037 | 0.017 | 0.042 | 0.052 | 0.058 | 0.048 | 0.006 | 0.043 | |
| VROCP6OXY1 | | | 0.037 | | | 0.075 | | 0.042 | | 0.091 | 0.059 | 0.066 | 0.074 | 0.14 | 0.096 | |
| OP3 | | 0.031 | 0.003 | | | 0.016 | | 0.011 | 0.015 | 0.007 | 0.004 | 0.051 | 0.061 | 0.022 | 0.032 | |

## S3.2 SOA yields from α-pinene

Under high-NO*x* conditions, the following reactions occur, leading to the formation of SOA from α-pinene (API).

| | |
|---|---|
| API + HO → 0.975 APIP1 + 0.025 APIP2 + … | SR24 (k =5.29×10$^{-11}$) |
| APIP1 + NO → 0.820 PINAL + 0.180 TRPN + … | SR25 (k = 4.00×10$^{-12}$) |
| APIP2 + NO → HOM + … | SR26 (k = 4.00×10$^{-11}$) |
| PINAL + HO → 0.230 PINALP + … | SR27 (k = 3.89×10$^{-11}$) |
| PINALP + NO → 0.050 TRPN + … | SR28 (k = 9.03×10$^{-12}$) |
| PINALP → HOM | SR29 (k=1.0 s$^{-1}$) |
| TRPN + HO → HOM | SR30 (k = 4.80×10$^{-11}$) |

HOM is the final non-volatile SOA product while other products (APIP1, APIP2, TPRN, PINAL, etc.) are all volatile. Similar to benzene case, we assumed [OH]=3.0×10$^6$ molecules/cm$^3$, [NO]=100 ppt, and [$HO_2$]= 1.5×10$^8$ molecules/cm$^3$ (=[OH] × 50) for the calculation of reaction rates. The SOA mass yield, specifically HOM, from API at time *t* is calculated as follows:

$$SOA_t = [HOM]_{t-1} + [TRPN]_{t-1} \cdot (1\text{-}e^{-k_{TRPN+OH}*[OH]*\Delta t}) \cdot \alpha_{TRPN}^{HOM} + [APIP2]_{t-1} \cdot (1\text{-}e^{-k_{APIP2+NO}*[NO]*\Delta t}) \cdot \alpha_{APIP2}^{HOM} + [PINALP]_{t-1} \cdot (1\text{-}e^{-k'_{PINALP\rightarrow HOM}*\Delta t}) \cdot \alpha'_{PINALP\rightarrow HOM} \quad \text{Eq. S4}$$

PINALP will either react with NO (SR28, k=9.03×10$^{-12}$ cm$^3$·molecule$^{-1}$·s$^{-1}$) or undergo auto-oxidation (SR29, k=1 s$^{-1}$). With [NO]=100 ppt, the reaction rate of SR28 is equal to 0.02 s$^{-1}$. We combine these two reactions to get:

$$k'_{PINALP\rightarrow HOM} = \frac{k_{auto-oxidation}}{k_{PINALP\rightarrow HOM} + k_{auto-oxidation}} \quad \text{Eq. S5}$$

$$\alpha'_{PINALP\rightarrow HOM} = \alpha_{auto-oxidation} \times \frac{k_{auto-oxidation}}{k_{PINALP\rightarrow HOM} + k_{auto-oxidation}} \quad \text{Eq. S6}$$

Figure S2a shows the yields of PINAL, TRPN, PINALP, and HOM as a function of aging time. As expected, both PINAL and PINALP undergo rapid reactions to produce TRPN, which subsequently leads to the formation of HOM. The SOA yields (i.e. HOM) experiences a significant increase during the initial six hours, after which the rate of increase becomes negligible. With a 24-hour aging period, the SOA yield from API is 0.599 g/g under high NO*x* conditions.

Additionally, we examined the sensitivity of SOA yields after a 24-hour aging period due to variations in NO concentration and the auto-oxidation rate. As illustrated by Figure S2b, SOA yield remains relatively stable until [NO] > 1000 ppt.

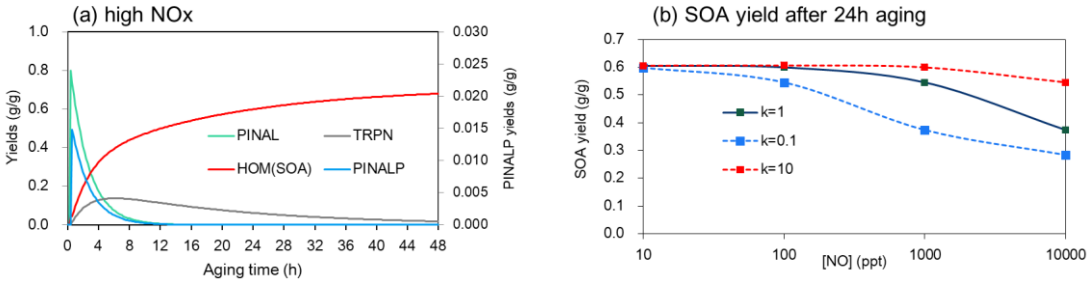


**Figure S2** (a) Yields of different species from API + OH as a function of aging time under high NO*x* conditions and (b) sensitivity of SOA yields to different [NO] and auto-oxidation rate.

Under low NO*x* conditions, SOA formation from API follows the following reaction:

API + HO → 0.975 APIP1 + 0.025 APIP2 + … SR31 (k =5.29×10$^{-11}$)

APIP1 + HO2 → OPB SR32 (k = 1.50×10$^{-11}$)

APIP2 + HO2 → HOM SR33 (k = 1.50×10$^{-11}$)

In this case, the SOA yield rapidly reaches a maximum value of 0.05 g/g after 1-hour

and stays the same afterwards (Figure S2b).

## Section S4. Box model configuration

### S4.1 Additional box model configuration details

The box model inputs and setup were developed from existing box model scenarios developed in a previous TCEQ project to compare chemical mechanisms for ozone (Ramboll, 2023). The modeling domain for the CAMx box model is 3 x 3 x 2 grid cells (in the x, y, and z dimensions). This is the smallest allowable CAMx domain since edge grid cells containing boundary conditions (BCs) are required by CAMx and 2 layers is the minimum allowed by the solution of vertical transport. All 9 grid cells in each layer have identical meteorological input data. The center grid cells of each domain, i.e. (2,2,1) and (2,2,2), form a 1-D column with layer 1 representing the planetary boundary layer (PBL) and layer 2 representing a residual layer between the PBL and the CAMx top. The PBL depth varies in time, as modeled by WRF for the TCEQ 2019 3-D CAMx modeling platform, whereas the top of layer 2 is constant in time at 3,000 m. Horizontal wind speeds in layer 1 are set to zero, preventing horizontal exchange between grid cells and ensuring BCs are not used to compute concentrations. In layer 2, there is a constant horizontal wind speed to purge the layer with a 12-hour lifetime to limit the accumulation of pollutants over time.

Simulations were conducted for a five-day period: September 3-7, 2019 for DFW and September 12-16, 2019 for TYL. CAMx box model input data (i.e., meteorology and initial conditions) were derived from the TCEQ 2019 3-D CAMx modeling platform. Since surface POA emissions were not included in the original model input, they were added by scaling to CO emissions using a scaling factor of 0.2. POA emissions are important because POA enhances SOA. These emissions result in average daily POA concentrations of 1.14 $\mu g/m^3$ at DFW and 0.21 $\mu g/m^3$ at Tyler.

### S4.2 SOA scheme fitting for CAMx box model

We implement four SOA schemes (i.e., CAMx SOAP2, CMAQ AERO7, CMAQ CRACMM, SIMPLE) in box model scenarios. While parameters of the existing CAMx SOAP2 can be directly adopted, the other three schemes need to develop

SOA yields that match with the SOAP2 structure. Development of these SOAP2-adjusted SOA yields for each scheme is described below.

### *S4.2.1 CMAQ AERO7 and CRACMM based schemes for CAMx*

The analysis of SOA yields as a function of ambient OA concentration ($C_{OA}$) (performed in Section S2 and S3) was leveraged to develop SOA schemes for CAMx that are similar to CMAQ's AERO7 and CRACMM. Curves were fit to the AERO7 and CRACMM data (Figure 3-Figure 5) for each SOA precursor using the SOAP2 C* values. The molar-based SOA yields in Table S11 through Table S14 provide good fits to the AERO7 and CRACMM data and are used in the new CAMx SOA schemes. Figure S3 shows an example fit for monoterpenes (TERP). The $R^2$ values for each fit range from 0.965 to 1.000 and the relative bias ranges from -1.6% to 3.3%. Since CRACMM has different chemical pathways for isoprene compared to CAMx, it was not possible to fit yield data. The values in Table S14 are therefore from the Simple scheme described below.

**Table S11** SOA molar-based yields from anthropogenic precursors under high (top) and low (bottom) NOx conditions for implementation of AERO7 based scheme into CAMx SOAP2

| | | | |
|---|---|---|---|
| C* [µg/m$^3$] @ 300K | 0 | 0.31 | 14 |
| CG/SOA MW [g/mol] | 220 | 150 | 160 |
| $\Delta H_{vap}$ [kJ/mol] | - | 18 | 18 |
| Benzene | 0.131 | 0.00 | 0.00 |
| | 0.004 | 0.00 | 0.187 |
| Toluene | 0.126 | 0.00 | 0.00 |
| | 0.00 | 0.012 | 0.092 |
| Xylene | 0.174 | 0.00 | 0.00 |
| | 0.005 | 0.00 | 0.064 |
| IVOC | 1.00 | 0.00 | 0.00 |
| | 1.00 | 0.00 | 0.00 |

**Table S12** SOA molar-based yields from biogenic precursors under high (top) and low (bottom) NO*x* conditions for implementation of AERO7 based scheme into CAMx SOAP2

| C* [µg/m$^3$] @ 300K | 0 | 0.45 | 26 |
|---|---|---|---|
| CG/SOA MW [g/mol] | 220 | 180 | 180 |
| $\Delta H_{vap}$ [kJ/mol] | - | 85 | 65 |
| Isoprene | 0.00 | 0.008 | 0.0038 |
| | 0.00 | 0.008 | 0.0038 |
| Monoterpene | 0.031 | 0.038 | 0.166 |
| | 0.031 | 0.038 | 0.166 |
| Sesquiterpene | 0.00 | 0.068 | 1.417 |
| | 0.00 | 0.068 | 1.417 |

**Table S13** SOA molar-based yields from anthropogenic precursors under high (top) and low (bottom) NO*x* conditions for implementation of CRACMM based scheme into CAMx SOAP2

| C* [µg/m$^3$] @ 300K | 0 | 0.31 | 14 |
|---|---|---|---|
| CG/SOA MW [g/mol] | 220 | 150 | 160 |
| $\Delta H_{vap}$ [kJ/mol] | - | 89 | 81 |
| Benzene | 0.142 | 0.141 | 0.00 |
| | 0.082 | 0.001 | 0.00 |
| Toluene | 0.126 | 0.160 | 0.00 |
| | 0.044 | 0.00 | 0.00 |
| Xylene | 0.005 | 0.304 | 0.778 |
| | 0.043 | 0.002 | 0.00 |
| IVOC | 0.00 | 0.117 | 0.583 |
| | 0.00 | 0.190 | 0.583 |

**Table S14** SOA molar-based yields from biogenic precursors under high (top) and low (bottom) NO*x* conditions for implementation of CRACMM based scheme into CAMx SOAP2

| C* [µg/m$^3$] @ 300K | 0 | 0.45 | 26 |
|---|---|---|---|
| CG/SOA MW [g/mol] | 220 | 180 | 180 |
| $\Delta H_{vap}$ [kJ/mol] | - | 85 | 81 |
| Isoprene | 0.01 | 0.00 | 0.00 |
| | 0.01 | 0.00 | 0.00 |
| Monoterpene | 0.028 | 0.00 | 0.00 |
| | 0.226 | 0.00 | 0.00 |
| Sesquiterpene | 0.009 | 0.963 | 0.873 |
| | 0.00 | 0.034 | 0.351 |

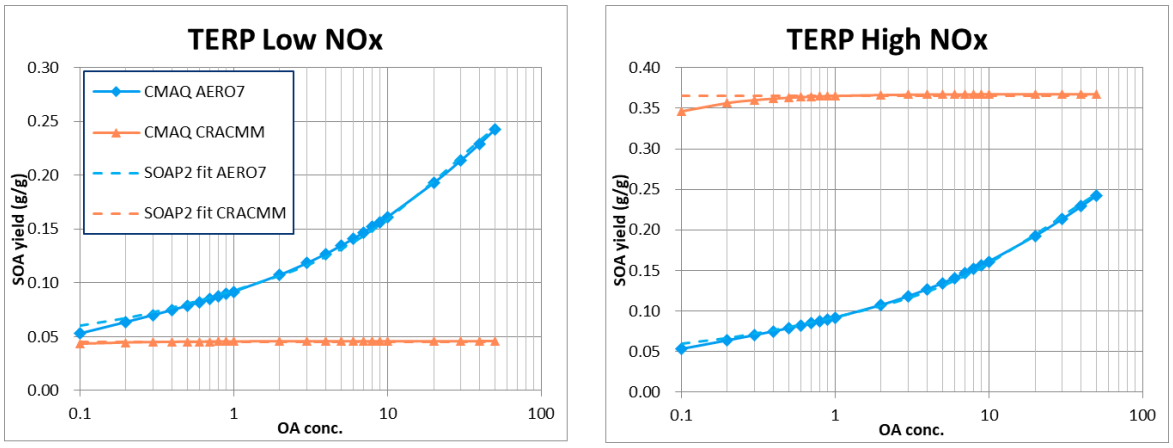


**Figure S3** SOA yields for terpenes under low and high NOx conditions for the AERO7 and CRACMM schemes (solid lines), and the corresponding fit (dashed lines) for the new schemes implemented in CAMx SOAP2.

### *S4.2.2 Simple scheme for CAMx*

The Simple scheme assumes all SOA formed is non-volatile. This is similar to the GEOS-Chem Simple scheme and the SOA scheme evaluated by Nault et al. (2021). The advantages to this scheme are that it is straightforward to implement, particularly with CAMx's source apportionment probing tools, and behaves more predictably and without nonlinearities present in other schemes. The SOA yields for the Simple scheme are provided in Table S15 and Table S16.The SOA yields for biogenic precursors are based on the literature review described in Section S1. The average SOA yield for each precursor species was calculated for an OA concentration ($C_{OA}$) of 10 µg/m$^3$ across different models (Table 2). 10 µg/m$^3$ is a relevant $C_{OA}$ to ambient air quality and often used as a reference for comparison. The high NO*x* SOA yields for isoprene, monoterpenes, and sesquiterpenes are the average yields from the following models/schemes: CAMx VBS, CMAQ AERO7, CMAQ CRACMM, GEOS-Chem Complex, CHIMERE VBS, and WRF-Chem MOSAIC. CAMx SOAP2 yields were excluded from the average since SOA aging is assumed in the yield values. Under low NO*x* conditions, the multi-model average SOA yields for the biogenic species are 25-55% larger than the high NO*x* yields. Considering this and the work by Sarrafzadeh et al. (2016) and Wildt et al. (2014), the low NO*x* yields in the new Simple scheme were set at 30% larger than the high NO*x* yields. This ensures a similar SOA behavior for all biogenic precursors at

493 different NO*x* levels.

494 The SOA yields for anthropogenic precursors are based on work by Seltzer et al.
495 (2021). High NO*x* yields for benzene, toluene, and xylene are provided by Seltzer et
496 al. (2021) and the IVOC yield is calculated by averaging the yields of the 15-carbon
497 species (including alkanes and PAHs) since IVOC is a 15-carbon species in CAMx.
498 The yields for toluene and xylene are comparable to the multi-model average from
499 the literature review, whereas the yields for benzene and IVOC are higher than the
500 multi-model average. Since benzene, toluene, and xylene are all aromatic species
501 with similar chemistry, they should behave similarly under varying NO*x* conditions.
502 The low NO*x* yields are therefore assumed to be two times higher than the high NOx
503 yields for the aromatics. For IVOC, low NO*x* yields are assumed to be 30% higher
504 than the high NO*x* yields. Both scaling factors are consistent with the literature
505 review results.

506 **Table S15** SOA molar-based yields from anthropogenic precursors under high
507 (top) and low (bottom) NO*x* conditions for implementation of the Simple scheme
508 into CAMx SOAP2

| | | | |
|---|---|---|---|
| C* [μg/m$^3$] @ 300K | 0 | 0.31 | 14 |
| CG/SOA MW [g/mol] | 220 | 150 | 160 |
| $\Delta H_{vap}$ [kJ/mol] | - | - | - |
| Benzene | 0.20 | 0.00 | 0.00 |
| | 0.10 | 0.00 | 0.00 |
| Toluene | 0.12 | 0.00 | 0.00 |
| | 0.06 | 0.00 | 0.00 |
| Xylene | 0.09 | 0.00 | 0.00 |
| | 0.04 | 0.00 | 0.00 |
| IVOC | 1.00 | 0.00 | 0.00 |
| | 1.00 | 0.00 | 0.00 |

**Table S16** SOA molar-based yields from biogenic precursors under high (top) and low (bottom) NO*x* conditions for implementation of the Simple based scheme into CAMx SOAP2

| | | | |
|---|---|---|---|
| C* [μg/m$^3$] @ 300K | 0 | 0.45 | 26 |
| CG/SOA MW [g/mol] | 220 | 180 | 180 |
| $\Delta H_{vap}$ [kJ/mol] | - | - | - |
| Isoprene | 0.01 | 0.00 | 0.00 |
| | 0.01 | 0.00 | 0.00 |
| Monoterpene | 0.10 | 0.00 | 0.00 |
| | 0.07 | 0.00 | 0.00 |
| Sesquiterpene | 0.40 | 0.00 | 0.00 |
| | 0.32 | 0.00 | 0.00 |

**Table S17** Initial and aged SOA yields (g/g) for CMAQ CRACMM IVOC types at 298 K and $C_{OA}$ of 10 μg/m$^3$. The aging effect is for 24-hour exposure to OH concentration of $3\times10^6$ molecules/cm$^3$.

| SOA yield | NO*x* condition | Alkane IVOC[1] | Emitted oxygenated IVOC | Aromatic IVOC[1] | Average[1] |
|---|---|---|---|---|---|
| Initial | High | 0.296 | 0.121 | 0.019 | 0.209 |
| | Low | 0.245 | 0.121 | 0.035 | 0.183 |
| Aged | High | 0.077 | 0.121 | 0.015 | 0.099 |
| | Low | 0.039 | 0.121 | 0.190 | 0.080 |

[1] Weighted average of ~C12 (ROCP6ALK), ~C14 (ROCP5ALK), ~C18 (ROCP4ALK), and ~C21 (ROCP3ALK) IVOC yields. Weighting factors for each IVOC category are adopted from Table S1 of Zhang et al., (2013).

[2] Arithmetic average of less volatile (ROCP5ARO) and more volatile aromatic (ROCP6ARO) IVOC yields.

[3]Aromatic IVOC are excluded from averaging due to disagreement with Pye et al. (2023) values.

## Section S5. Additional figures and tables

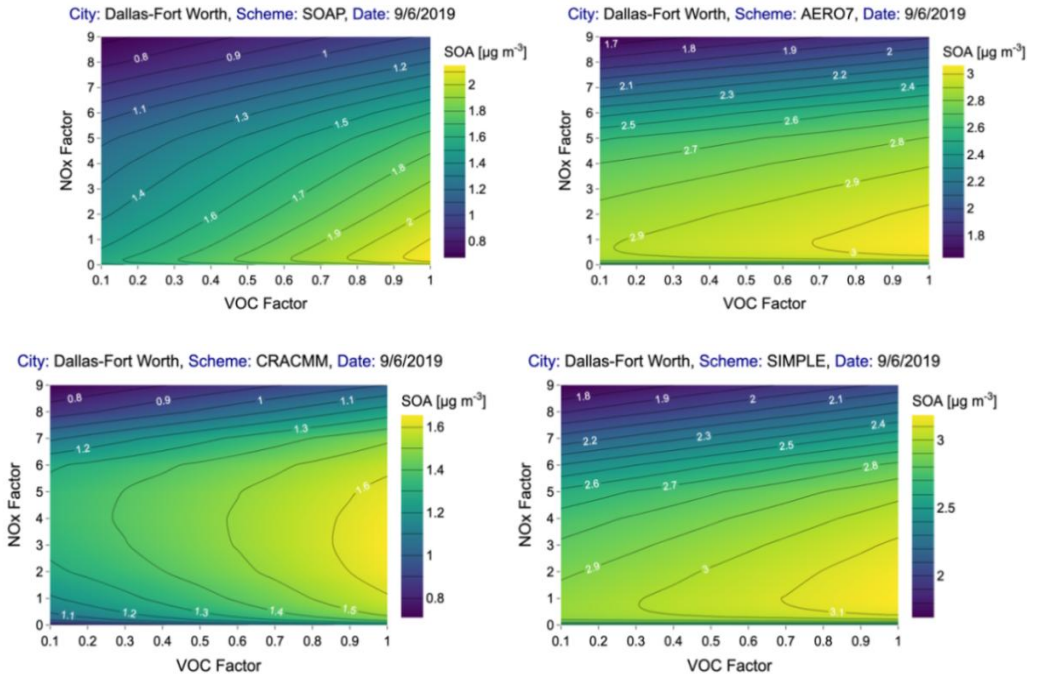


**Figure S4** SOA response surface (24-hr average, µg/m$^3$) to varying anthropogenic NO*x* and VOC emissions for DFW for four different SOA schemes. NO*x* and VOC scaling factors of 1 are the base case simulation. Note that the concentration scale is different for each scheme.

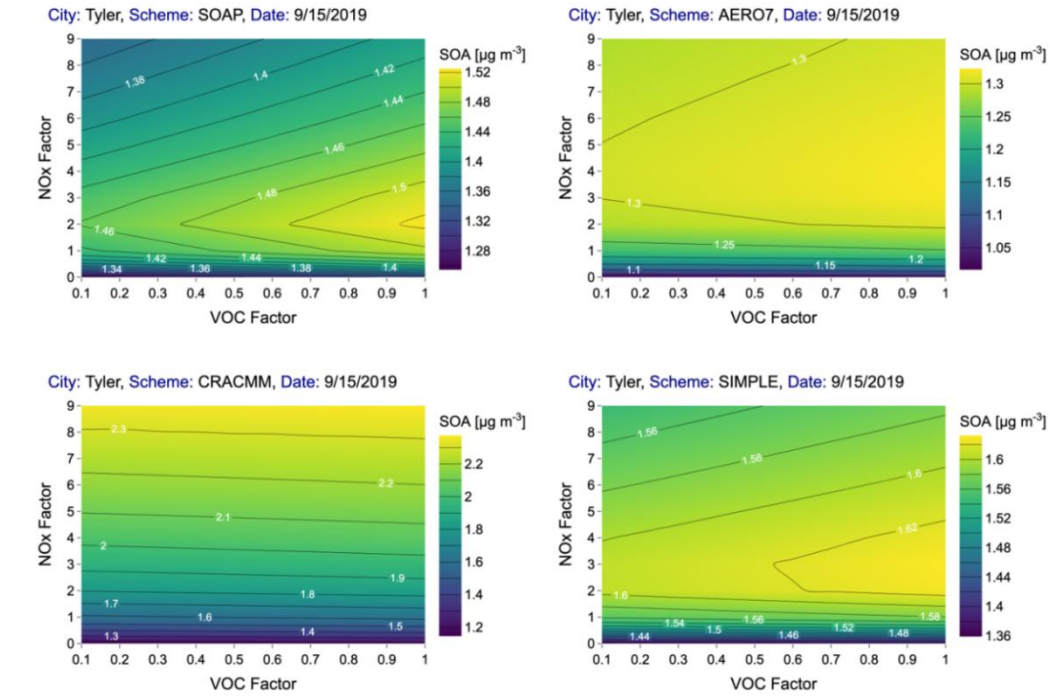


**Figure S5** SOA response surface (24-hr average, µg/m$^3$) to varying anthropogenic NO*x* and VOC emissions for TYL for four different SOA schemes. NO*x* and VOC scaling factors of 1 are the base case simulation. Note that the concentration scale is different for each scheme.

**Table S18** Ratio of non-aged high to low NO*x* SOA yields for different precursors in each scheme. Values in bold italics indicate higher yields under high NO*x* conditions (ref. Table 1 for specific numbers).

| Precursor | CAMx | | CMAQ | | GEOS-Chem | | CHIMERE | WRF-Chem |
|---|---|---|---|---|---|---|---|---|
| | SOAP2 | VBS | AERO7 | CRACMM | Simple | Complex | VBS | MOSAIC |
| BENZ | ***1.25*** | 0.53 | 0.39 | / | / | 0.39 | 0.54 | 0.89 |
| TOL | 0.52 | 0.90 | 0.27 | / | / | 0.28 | 0.54 | 0.89 |
| XYL | 0.16 | 0.51 | 0.14 | / | / | 0.14 | 0.51 | 0.89 |
| IVOC | 0.65 | 1.00 | 1.00 | / | / | 0.28 | 1.00 | 1.00 |
| ISOP | 0.52 | 0.47 | 1.00 | / | 1.00 | 1.00 | 0.53 | 0.56 |
| TERP | 0.67 | 0.52 | 1.00 | / | 1.00 | 0.50 | 0.53 | 0.52 |
| SESQ | 0.74 | 1.00 | 1.00 | / | 1.00 | ***2.00*** | 1.00 | 1.00 |

**Table S19** Ratio of aged high to low NO*x* SOA yields for different precursors in each scheme. Values in bold italics indicate higher yields under low NO*x* conditions (ref. Table 2 for specific numbers).

| Precursor | CAMx | | CMAQ | | GEOS-Chem | | CHIMERE | WRF-Chem |
|---|---|---|---|---|---|---|---|---|
| | SOAP2 | VBS | AERO7 | CRACMM | Simple | Complex | VBS | MOSAIC |
| BENZ | ***1.25*** | 0.75 | 0.61 | 0.35 | / | 0.39 | 0.71 | 0.89 |
| TOL | 0.52 | 0.98 | 0.41 | 0.21 | / | 0.28 | 0.71 | 0.89 |
| XYL | 0.16 | 0.72 | 0.20 | 0.18 | / | 0.14 | 0.68 | 0.89 |
| IVOC | 0.65 | 1.00 | 1.00 | 0.59 | / | 0.28 | 1.00 | 1.00 |
| ISOP | 0.52 | 0.47 | 1.00 | / | 1.00 | 1.00 | 0.66 | 0.56 |
| TERP | 0.67 | 0.52 | 1.00 | ***4.30*** | 1.00 | 0.50 | 0.67 | 0.52 |
| SESQ | 0.74 | 1.00 | 1.00 | 0.51 | 1.00 | ***2.00*** | 1.00 | 1.00 |

**Table S20** Average concentrations (μg/m$^3$) of anthropogenic SOA (ASOA) and biogenic SOA (BSOA) over days 2 through 5 for the base and reduced NO*x* model simulations. Values in bold italics indicates a decrease in SOA concentrations in the reduced NO*x* model runs compared to the base runs.

| | SOAP2 | | | AERO7 | | | CRACMM | | | Simple | | |
|---|---|---|---|---|---|---|---|---|---|---|---|---|
| | Base | 50% NO*x* | Diff (%) | Base | 50% NO*x* | Diff (%) | Base | 50% NO*x* | Diff (%) | Base | 50% NO*x* | Diff (%) |
| DFW | | | | | | | | | | | | |
| ASOA | 1.34 | 1.48 | 9.6% | 2.34 | 2.38 | 1.9% | 0.78 | 0.81 | 3.5% | 2.44 | 2.45 | 0.6% |
| BSOA | 0.42 | 0.48 | 12.2% | 0.41 | 0.42 | 0.4% | 0.65 | 0.59 | ***-10.7%*** | 0.45 | 0.46 | 2.4% |
| Total SOA | 1.76 | 1.96 | 10.3% | 2.75 | 2.80 | 1.6% | 1.43 | 1.40 | ***-2.5%*** | 2.88 | 2.91 | 0.9% |
| TYL | | | | | | | | | | | | |
| ASOA | 0.24 | 0.25 | 4.4% | 0.28 | 0.31 | 9.9% | 0.16 | 0.17 | 1.0% | 0.30 | 0.32 | 8.5% |
| BSOA | 1.19 | 1.14 | ***-4.1%*** | 0.87 | 0.82 | ***-6.2%*** | 1.40 | 1.24 | ***-12.6%*** | 1.19 | 1.14 | ***-4.4%*** |
| Total SOA | 1.43 | 1.40 | ***-2.5%*** | 1.16 | 1.14 | ***-1.8%*** | 1.56 | 1.41 | ***-11.0%*** | 1.49 | 1.46 | ***-1.5%*** |

**Table S21** Ratio of aged SOA yields (Table 3) to non-aged SOA yields (Table 2) from different precursors simulated by different schemes. Bold font values indicate no aging processes implemented.

| Precursor-NOx case | CMx[1] SP2 | CMx VBS | CMQ AE7 | CMQ CRM[1] | G-C Spl | G-C Cpx | CMR VBS | W-C MOS | Avg[2] |
|---|---|---|---|---|---|---|---|---|---|
| BENZ-high | **1.0** | 6.9 | 1.6 | / | **1.0** | **1.0** | 4.1 | **1.0** | 2.4 |
| BENZ-low | **1.0** | 4.9 | **1.0** | / | **1.0** | **1.0** | 3.1 | **1.0** | 1.9 |
| TOL-high | **1.0** | 6.9 | 1.5 | / | **1.0** | **1.0** | 4.1 | **1.0** | 2.4 |
| TOL-low | **1.0** | 6.3 | **1.0** | / | **1.0** | **1.0** | 3.1 | **1.0** | 2.1 |
| XYL-high | **1.0** | 6.3 | 1.5 | / | **1.0** | **1.0** | 3.9 | **1.0** | 2.2 |
| XYL-low | **1.0** | 4.4 | **1.0** | / | **1.0** | **1.0** | 2.9 | **1.0** | 1.8 |
| IVOC high | **1.0** | 2.2 | **1.0** | / | / | **1.0** | 60 | 4448 | 645 |
| IVOC-low | **1.0** | 2.2 | **1.0** | / | / | **1.0** | 60 | 4448 | 645 |
| ISOP-high | **1.0** | **1.0** | 1.3 | / | **1.0** | **1.0** | 2.3 | **1.0** | 1.2 |
| ISOP-low | **1.0** | **1.0** | 1.3 | / | **1.0** | **1.0** | 1.8 | **1.0** | 1.2 |
| TERP-high | **1.0** | **1.0** | **1.0** | / | **1.0** | **1.0** | 4.1 | **1.0** | 1.4 |
| TERP-low | **1.0** | **1.0** | **1.0** | / | **1.0** | **1.0** | 3.2 | **1.0** | 1.3 |
| SESQ-high | **1.0** | **1.0** | 1.8 | / | **1.0** | **1.0** | 4.2 | **1.0** | 1.6 |
| SESQ-low | **1.0** | **1.0** | 1.8 | / | **1.0** | **1.0** | 4.2 | **1.0** | 1.6 |

[1] Ratio for CRACMM is not applicable as the initial SOA yields are zero.

[2] Excluding CRACMM.

549 **Table S22** Ranking (from lowest to highest) initial SOA yields from different
550 precursors by each scheme under high and low NO*x* conditions (ref. Table 2 for
551 specific numbers)

| Ranking | CAMx SOAP2 | CAMx VBS | CMAQ AERO7 | CMAQ CRAMM | GOES-Chem Simple | GEOS-Chem Complex | CHIMERE VBS | WRF-Chem MOSAIC |
|---|---|---|---|---|---|---|---|---|
| *High NOx conditions* | | | | | | | | |
| 1 | ISOP | ISOP | ISOP | | ISOP | ISOP | IVOC | IVOC |
| 2 | Xylene | TERP | Xylene | | TERP | Xylene | ISOP | ISOP |
| 3 | TERP | Benzene | Toluene | | SESQ | Toluene | TERP | TERP |
| 4 | IVOC | Xylene | Benzene | | | TERP | Xylene | Benzene |
| 5 | Toluene | Toluene | TERP | | | Benzene | Benzene | Toluene |
| 6 | Benzene | SESQ | SESQ | | | IVOC | Toluene | Xylene |
| 7 | SESQ | IVOC | IVOC | | | SESQ | SESQ | SESQ |
| *Low NOx conditions* | | | | | | | | |
| 1 | ISOP | ISOP | ISOP | | ISOP | ISOP | IVOC | IVOC |
| 2 | TERP | TERP | TERP | | TERP | TERP | ISOP | ISOP |
| 3 | Benzene | Toluene | Toluene | | SESQ | Toluene | SESQ | TERP |
| 4 | IVOC | SESQ | Xylene | | | Xylene | TERP | Benzene |
| 5 | SESQ | Benzene | Benzene | | | Benzene | Xylene | Toluene |
| 6 | Xylene | Xylene | SESQ | | | SESQ | Benzene | Xylene |
| 7 | Toluene | IVOC | IVOC | | | IVOC | Toluene | SESQ |

552

**Table S23** Ranking (from lowest to highest) aged SOA yields from different precursors by each scheme under high and low NO*x* conditions (ref. Table 3 for specific numbers)

| Ranking | CAMx SOAP2 | CAMx VBS | CMAQ AERO7 | CMAQ CRAMM | GOES-Chem Simple | GEOS-Chem Complex | CHIMERE VBS | WRF-Chem MOSAIC |
|---|---|---|---|---|---|---|---|---|
| *High NOx conditions* | | | | | | | | |
| 1 | ISOP | ISOP | ISOP | Xylene | ISOP | ISOP | IVOC | ISOP |
| 2 | Xylene | TERP | Xylene | Toluene | TERP | Xylene | ISOP | TERP |
| 3 | TERP | SESQ | Toluene | Benzene | SESQ | Toluene | TERP | Benzene |
| 4 | IVOC | Benzene | TERP | IVOC | | TERP | Xylene | Toluene |
| 5 | Toluene | Xylene | Benzene | SESQ | | Benzene | Benzene | Xylene |
| 6 | Benzene | IVOC | SESQ | TERP | | IVOC | Toluene | SESQ |
| 7 | SESQ | Toluene | IVOC | | | SESQ | SESQ | IVOC |
| *Low NOx conditions* | | | | | | | | |
| 1 | ISOP | ISOP | ISOP | TERP | ISOP | ISOP | IVOC | ISOP |
| 2 | TERP | TERP | TERP | Toluene | TERP | TERP | ISOP | TERP |
| 3 | Benzene | SESQ | Toluene | Xylene | SESQ | Toluene | TERP | Benzene |
| 4 | IVOC | Benzene | Xylene | IVOC | | Xylene | SESQ | Toluene |
| 5 | SESQ | Xylene | Benzene | Benzene | | Benzene | Xylene | Xylene |
| 6 | Xylene | IVOC | SESQ | SESQ | | SESQ | Benzene | SESQ |
| 7 | Toluene | Toluene | IVOC | | | IVOC | Toluene | IVOC |

## References


Appel, K. W., Bash, J. O., Fahey, K. M., Foley, K. M., Gilliam, R. C., Hogrefe, C., and Wong, D. C.: The Community Multiscale Air Quality (CMAQ) model versions 5.3 and 5.3.1: system updates and evaluation, Geoscientific Model Development, 14, 2867-2897, 2021.

Beekmann, M. and Vautard, R.: A modelling study of photochemical regimes over Europe: robustness and variability, Atmospheric Chemistry and Physics, 10, 10067-10084, 2010.

CHIMERE Users Guide: https://www.lmd.polytechnique.fr/chimere/, 2023.

Cholakian, A., Beekmann, M., Colette, A., Coll, I., Siour, G., Sciare, J., and Dulac, F.: Simulation of fine organic aerosols in the western Mediterranean area during the ChArMEx 2013 summer campaign, Atmospheric Chemistry and Physics, 18, 7287-7312, 2018.

Couvidat, F., Bessagnet, B., Garcia-Vivanco, M., Real, E., Menut, L., and Colette, A.: Development of an inorganic and organic aerosol model (CHIMERE 2017 β v1.0): Seasonal and spatial evaluation over Europe, Geoscientific Model Development, 11, 165-194, 2018.

Hodzic, A. and Jimenez, J. L.: Modeling anthropogenically controlled secondary organic aerosols in a megacity: A simplified framework for global and climate models, Geoscientific Model Development, 4, 901-917, 2011.

Hodzic, A. and Jimenez, J. L.: Modeling anthropogenically controlled secondary organic aerosols in a megacity: A simplified framework for global and climate models, Geoscientific Model Development, 4, 901-917, 2011.

Hodzic, A., Jimenez, J. L., Madronich, S., Aiken, A. C., Bessagnet, B., Curci, G., and Ulbrich, I. M.: Modeling organic aerosols during MILAGRO: application of the CHIMERE model and importance of biogenic secondary organic aerosols, Atmospheric Chemistry and Physics Discussions, 9, 12207-12281, 2009.

Hodzic, A., Jimenez, J. L., Madronich, S., Canagaratna, M. R., DeCarlo, P. F., Kleinman, L., and Fast, J.: Modeling organic aerosols in a megacity: potential contribution of semi-volatile and intermediate volatility primary organic compounds to secondary organic aerosol formation, Atmospheric Chemistry and Physics, 10, 5491-5514, 2010.

Hodzic, A., Kasibhatla, P. S., Jo, D. S., Cappa, C. D., Jimenez, J. L., Madronich, S., and Park, R. J.: Rethinking the global secondary organic aerosol (SOA) budget: stronger production, faster removal, shorter lifetime, Atmospheric Chemistry and Physics, 16, 7917-7941, 2016.

Honoré, C., Rouil, L., Vautard, R., Beekmann, M., Bessagnet, B., Dufour, A., and Poisson, N.: Predictability of European air quality: Assessment of 3 years of

operational forecasts and analyses by the PREV'AIR system, Journal of Geophysical Research: Atmospheres, 113, 2008.

Koo, B., Knipping, E., and Yarwood, G.: 1.5-Dimensional volatility basis set approach for modeling organic aerosol in CAMx and CMAQ, Atmospheric Environment, 95, 158-164, 2014.

Lane, T. E., Donahue, N. M., and Pandis, S. N.: Simulating secondary organic aerosol formation using the volatility basis-set approach in a chemical transport model, Atmospheric Environment, 42, 7439-7451, 2008.

Luecken, D. J., Phillips, S., Sarwar, G., and Jang, C.: Effects of using the CB05 vs. SAPRC99 vs. CB4 chemical mechanism on model predictions: Ozone and gas-phase photochemical precursor concentrations, Atmospheric Environment, 42, 5805-5820, 2008.

Ma, S., Zhang, X., Gao, C., Tong, Q., Xiu, A., Zhao, H., and Zhang, S.: Simulating performance of CHIMERE on a late autumnal dust storm over Northern China, Sustainability, 11, 1074, 2019.

Marais, E. A., Jacob, D. J., Jimenez, J. L., Campuzano-Jost, P., Day, D. A., Hu, W., and McNeill, V. F.: Aqueous-phase mechanism for secondary organic aerosol formation from isoprene: application to the southeast United States and co-benefit of SO2 emission controls, Atmospheric Chemistry and Physics, 16, 1603-1618, 2016.

Murphy, B. N. and Pandis, S. N.: Simulating the formation of semivolatile primary and secondary organic aerosol in a regional chemical transport model, Environmental Science & Technology, 43, 4722-4728, 2009.

Murphy, B. N., Woody, M. C., Jimenez, J. L., Carlton, A. M. G., Hayes, P. L., Liu, S., and Pye, H. O.: Semivolatile POA and parameterized total combustion SOA in CMAQv5.2: impacts on source strength and partitioning, Atmospheric Chemistry and Physics, 17, 11107-11133, 2017.

Nault, B. A., Jo, D. S., McDonald, B. C., Campuzano-Jost, P., Day, D. A., Hu, W., Schroder, J. C., Allan, J., Blake, D. R., Canagaratna, M. R., and Coe, H.: Secondary organic aerosols from anthropogenic volatile organic compounds contribute substantially to air pollution mortality, Atmospheric Chemistry and Physics, 21, 11201-11224, 2021.

Pai, S. J., Heald, C. L., Pierce, J. R., Farina, S. C., Marais, E. A., Jimenez, J. L., and Vu, K.: An evaluation of global organic aerosol schemes using airborne observations, Atmospheric Chemistry and Physics, 20, 2637-2665, 2020.

Pye, H. O. T., Chan, A. W. H., Barkley, M. P., and Seinfeld, J. H.: Global modeling of organic aerosol: the importance of reactive nitrogen (NOx and NO3), Atmospheric Chemistry and Physics, 10, 11261-11276, 2010.

Pye, H. O., Place, B. K., Murphy, B. N., Seltzer, K. M., D'Ambro, E. L., Allen, C., and Stockwell, W. R.: Linking gas, particulate, and toxic endpoints to air

emissions in the Community Regional Atmospheric Chemistry Multiphase Mechanism (CRACMM), Atmospheric Chemistry and Physics, 23, 5043-5099, 2023.

CAMx User's Guide, Version 7.20: https://www.camx.com/download/source/, 2024.

Robinson, A. L., Donahue, N. M., Shrivastava, M. K., Weitkamp, E. A., Sage, A. M., Grieshop, A. P., and Pandis, S. N.: Rethinking organic aerosols: Semivolatile emissions and photochemical aging, Science, 315, 1259-1262, 2007.

Sarrafzadeh, M., Wildt, J., Pullinen, I., Springer, M., Kleist, E., Tillmann, R., Schmitt, S. H., Wu, C., Mentel, T. F., Zhao, D., and Hastie, D. R.: Impact of NOx and OH on secondary organic aerosol formation from β-pinene photooxidation, Atmospheric Chemistry and Physics, 16, 11237-11248, 2016.

Schell, B., Ackermann, I. J., Hass, H., Binkowski, F. S., and Ebel, A.: Modeling the formation of secondary organic aerosol within a comprehensive air quality model system, Journal of Geophysical Research: Atmospheres, 106, 28275-28293, 2001.

Sciare, J., d'Argouges, O., Zhang, Q. J., Sarda-Estève, R., Gaimoz, C., Gros, V., and Sanchez, O.: Comparison between simulated and observed chemical composition of fine aerosols in Paris (France) during springtime: contribution of regional versus continental emissions, Atmospheric Chemistry and Physics, 10, 11987-12004, 2010.

Shrivastava, M., Easter, R. C., Liu, X., Zelenyuk, A., Singh, B., Zhang, K., and Tiitta, P.: Global transformation and fate of SOA: Implications of low - volatility SOA and gas - phase fragmentation reactions, Journal of Geophysical Research: Atmospheres, 120, 4169-4195, 2015.

Shrivastava, M., Fast, J., Easter, R., Gustafson Jr, W. I., Zaveri, R. A., Jimenez, J. L., and Hodzic, A.: Modeling organic aerosols in a megacity: comparison of simple and complex representations of the volatility basis set approach, Atmospheric Chemistry and Physics, 11, 6639-6662, 2011.

Strader, R., Lurmann, F., and Pandis, S. N.: Evaluation of secondary organic aerosol formation in winter, Atmospheric Environment, 33, 4849-4863, 1999.

Wildt, J., Mentel, T. F., Kiendler-Scharr, A., Hoffmann, T., Andres, S., Ehn, M., Kleist, E., Müsgen, P., Rohrer, F., Rudich, Y., and Springer, M.: Suppression of new particle formation from monoterpene oxidation by NOx, Atmospheric Chemistry and Physics, 14, 2789-2804, 2014.

WRF-Chem version 4.4 Users Guide: https://ruc.noaa.gov/wrf/wrf-chem/Users_guide.pdf, 2022 .

Zhang, Q., Laurent, B., Velay-Lasry, F., Ngo, R., Derognat, C., Marticorena, B., and Albergel, A.: An air quality forecasting system in Beijing-Application to the

675 study of dust storm events in China in May 2008, Journal of Environmental
676 Sciences, 24, 102-111, 2012.

677 Zhang, Q. J., Beekmann, M., Drewnick, F., Freutel, F., Schneider, J., Crippa, M.,
678 and Perrussel, O.: Formation of organic aerosol in the Paris region during the
679 MEGAPOLI summer campaign: evaluation of the volatility-basis-set
680 approach within the CHIMERE model, Atmospheric Chemistry and Physics,
681 13, 5767-5790, 2013.

682